Available Online

JSR Publications

J. Sci. Res. **15** (3), 621-636 (2023)

JOURNAL OF SCIENTIFIC RESEARCH

www.banglajol.info/index.php/JSR

Unsteady Williamson Fluid Flow Over Exponentially Stretching Sheet in the presence of Non-Uniform Heat Generation or Absorption and Inclined Magnetic Field

R. Akter*, M. A. Islam

Department of Natural Science, Port City International University, Chattogram, 4217, Bangladesh

Received 26 December 2022, accepted in final revised form 5 March 2023

Abstract

The effect of an inclined magnetic field on unsteady magneto hydrodynamic Williamson fluid flow past an exponentially stretching sheet with joule heating, non-uniform heat generation or absorption, and suction or blowing is investigated numerically in this work. The reduced non-linear ordinary differential equations are obtained from governing partial differential equations using appropriate similarity transformations. The reduced equations are then solved with the help of bvp4c in MATLAB. The effects of various physical parameters on velocity, temperature and concentration profile, skin friction coefficient, Nusselt, and Sherwood number are described through graphs and tables. The result indicates that the rising values of the Weissenberg number decrease the velocity profile and increase the temperature and concentration profiles. It is also found that an inclined magnetic field reduces fluid velocity.

Keywords: Williamson fluid; Non-uniform heat generation or absorption; Joule heating; Inclined magnetic field; Unsteady.

doi: http://doi.org/10.3329/jsr.v15i3.63523 J. Sci. Res. **15** (3), 621-636 (2023)

1. Introduction

Fluids that don't follow Newton's law of viscosity are known as non-Newtonian fluid, which has notable applications in manufacturing and processing industries. Pseudo-plastic fluids, which are shear-thinning fluids, are the most often encountered fluid in the case of non-Newtonian fluids. Since the rheological properties of these fluids can't be illustrated through Navier-stokes equations alone, many rheological models like the Carreau, Ellis, Jeffrey, Maxwell, and Power law models have been established to overcome this task. The Williamson fluid model, considered by Williamson in 1929, is another influential model used to describe the rheological properties of pseudo-plastic fluids [1]. Babu and Sandeep [2] described the cross-diffusion effects on MHD Williamson fluid flow in the presence of Soret and Dufour and found that fluid temperature reduces while the concentration profile increases with large values of Soret and Dufour number, respectively. Shah *et al.* [3] investigated the problem of unsteady MHD liquid thin film flow of Williamson fluid with

* *Corresponding author*: tromenaakter@gmail.com

the effects of thermal radiation over a porous stretching surface numerically and found that the temperature profile is an increasing function of radiation parameter and porosity parameter declines the flow of thin films. Lund *et al.* [4] described double slip effects on MHD mixed convection flow and heat transfer of Williamson fluid past an exponentially stretching or shrinking sheet and found that both velocity and thermal slip parameters reduce fluid velocity and temperature, respectively. Salahuddin *et al.* [5] examined the induced magnetic field effects on the boundary layer flow of Williamson fluid with variable viscosity, conductivity, and diffusivity. Ellahi [6] studied non-Newtonian nanofluid in a pipe with the effects on MHD and variable viscosity. Ellahi *et al.* [7] explored the problem of steady MHD boundary layer flow and heat transfer over a flat plate with entropy analysis and velocity slip at the boundary. Shehzad *et al.* [8] analytically inspected the convective fluid of multilayer Newtonian and non-Newtonian fluid coatings through parallel inclined plates. Nowadays, the study of joule heating and heat generation or absorption has attracted researchers due to its vast application in engineering and industry. There are generally two types of internal heat generation/absorption: one is dependent on temperature, while the other is dependent on temperature and space. This study considers temperature and space-dependent heat generation/absorption, known as non-uniform heat generation/absorption. Heat generation/absorption has enormous applications in metal waste, nuclear reactor engineering, chillers, combustion engineering, and heat pumps [9-10]. Joule heating is produced by intercommunication among the atomic ions that compose the conductor's body and moving charged particles that form the current. It is a result of the impingement between the moving particles. Joule heating has many practical uses, such as electric stoves and other electric heaters, soldering irons, cartridge heaters, electric fuses, electronic cigarettes, thermistors, food processing equipment, etc. [11]. Sinha *et al.* [12] theoretically analyzed the problem of unsteady MHD blood flow and heat transfer in a permeable vessel in the presence of non-uniform heat generation/absorption. Swain *et al.* [13] illustrated the MHD flow and gradient heat transport of a Newtonian fluid over a stretching sheet embedded in a porous medium with joule heating and non-uniform heat source/sink effects. Hayat *et al.* [14] discussed the effects of joule heating on MHD two-dimensional flow and heat transfer of Williamson fluid over a stretching sheet with viscous dissipation. Sharada and Shankar [15] studied the problem of MHD mixed convective flow of Williamson fluid in joule heating with velocity slip and thermal convective boundary conditions. Hamid *et al.* [16] explored the effect of joule heating on the unsteady MHD stagnation point flow of Williamson fluid over a stretching/shrinking sheet in the presence of viscous dissipation and suction.

The flow field can be significantly changed due to the suction or blowing of a fluid, which is important in many engineering activities, such as the design of thrust bearing and radial diffusers and thermal oil recovery. n general, suction has a tendency to enhance skin friction, whereas the reverse is seen for blowing. Injection or withdrawal of fluid through a porous bounding wall is of general interest in practical problems involving boundary layer control applications such as film cooling, polymer fiber coating, and coating of

wires. Reactants can be removed from chemical processes employing suction, whereas blowing is applied to add reactants, cool the surface, stop corrosion or scaling, and decrease the drag [17]. Recently, Islam *et al*. [18] analyzed numerically the multiple slip effects on unsteady MHD flow over an exponentially stretching sheet in a porous medium with suction or blowing. Later, Islam *et al*. [19] discussed the problem of unsteady MHD mixed convection heat and mass transfer slip flow with suction/blowing in the presence of radiation and heat generation or absorption and found that suction increases fluid velocity, temperature, and concentration while the opposite trend is seen for blowing.

In light of the literature mentioned above, the present paper aims to analyze the unsteady magnetohydrodynamic (MHD) boundary layer flow of Williamson fluid due to an exponentially stretching sheet with suction or blowing in the presence of joule heating and non-uniform heat source or sink. The governing boundary layer equations are transformed into a two-point boundary value problem in similarity variables, and the resultant problem is solved numerically using the bvp4c solver in MATLAB. The effects of various governing parameters on the fluid velocity, temperature, concentration, and Nusselt number are shown in Figs and analyzed in detail. The skin friction coefficient, Nusselt number, and Sherwood number are computed and examined.

2. Mathematical Formulation of the Problem

Consider a laminar, unsteady, incompressible two dimensional, and electrically conducting flow of Williamson fluid over a stretching sheet along the x axis while the y axis is normal to it. The sheet is stretched exponentially with the velocity $U = \frac{U_0 e^{x/L}}{1-\alpha t}$, where $U_0 > 0$ is a stretching rate along the x axis.

The Cauchy stress tensor for Williamson fluid flow is defined as follows [20]:

$$S = -pI + \tau \tag{1}$$

where p is the pressure, I is the identity tensor, $\tau = \left(\mu_\infty + \frac{\mu_0 - \mu_\infty}{1-\Gamma\gamma}\right) A_1$ denotes the extra shear tensor, μ_0 is the limiting viscosity at zero shear rates, μ_∞ is the limiting viscosity at the infinite shear rate, $\Gamma > 0$ is a time constant, A_1 is the first Rivlin-Ericksen tensor, and γ is defined as follows:

$$\gamma = \sqrt{\frac{1}{2}\,\pi}, \pi = trace(A_1^2), \gamma = \left\{\left(\frac{\partial u}{\partial y}\right)^2 + \frac{1}{2}\left(\frac{\partial u}{\partial y} + \frac{\partial v}{\partial x}\right)^2 + \left(\frac{\partial v}{\partial y}\right)^2\right\}^{\frac{1}{2}}.$$

Considering $\mu_\infty = 0$ and $\Gamma\gamma < 1$, we get $\tau = \frac{\mu_0}{1-\Gamma\gamma} A_1$. Expanding this expression in powers of $\Gamma\gamma$ and taking only linear terms, we get $\tau = \mu_0 (1 + \Gamma\gamma) A_1$. Then equation (1) becomes

$$S = -pI + \mu_0 (1 + \Gamma\gamma) A_1$$

We can write the governing equations of the flow field as follows:

$$\frac{\partial u}{\partial x} + \frac{\partial v}{\partial y} = 0 \tag{2}$$

$$\frac{\partial u}{\partial t}+u\frac{\partial u}{\partial x}+v\frac{\partial u}{\partial y}=\nu\frac{\partial^2 u}{\partial y^2}+\sqrt{2}\,\nu\,\Gamma\frac{\partial u}{\partial y}\ \ \frac{\partial^2 u}{\partial y^2}-\frac{\sigma B^2}{\rho}u\,sin^2\psi \tag{3}$$

$$\frac{\partial T}{\partial t}+u\frac{\partial T}{\partial x}+v\frac{\partial T}{\partial y}=\frac{\kappa}{\rho\,C_p}\frac{\partial^2 T}{\partial y^2}+\frac{\sigma B^2}{\rho}u^2\ +\frac{1}{\rho\,C_p}q''' \tag{4}$$

$$\frac{\partial C}{\partial t}+u\frac{\partial C}{\partial x}+v\frac{\partial C}{\partial y}=D_m\frac{\partial^2 C}{\partial y^2} \tag{5}$$

with the boundary conditions

$$u=U(x,t)\ ,\quad V=-V(x,t),T=T_w(x,t)\ ,C=C_w(x,t)\ ,at\ y=0$$
$$u\to 0,T\to T_\infty,C\to C_\infty\quad as\ y\to\infty \tag{6}$$

Here u and v are the velocity components along the x axis and y axis, respectively, t is the time, $\nu\ (=\mu/\rho)$ is the kinematic fluid viscosity, μ is the co-efficient of fluid viscosity, ρ is the density, $\Gamma>0$ is the time constant, σ is the electric conductivity of the fluid, T is the temperature of the fluid, κ is the thermal conductivity, C_p is the specific heat at constant pressure, C is the concentration of the fluid and D_m is the co-efficient of mass diffusivity.

The time-dependent non-uniform heat generation or absorption q''' is defined as

$$q'''=\frac{K\,U}{L\,\nu}\ [A_1\ (T_W-T_\infty)\,f'+B_1(T-T_\infty)] \tag{7}$$

Here $A_1,B_1>0$ implies heat generation and $A_1,B_1<0$ implies heat absorption.

For the solution of momentum, energy, and concentration equations (3), (4), and (5), we introduce the following dimensionless variables:

$$\eta=\sqrt{\frac{U}{2\,\nu L}}\ y\,,\qquad \psi=\sqrt{2\nu L\,U}\,f(\eta)$$

$$T=T_\infty+\frac{T_0}{(1-\alpha t)^2}e^{x/2L}\ \theta(\eta),\ C=C_\infty+\frac{C_0}{(1-\alpha t)^2}e^{x/2L}\,\phi(\eta)$$

Introducing dimensionless similarity variables into the governing equations (3)-(5), we get the following system of ordinary differential equations:

$$f'''(1+We\,f'')+\ f\,f''-2\,f'^2-A\,e^{-X}\,(2f'+\eta\,f'')-Msin^2\psi\,f'=0 \tag{8}$$

$$\theta''+\mathrm{Pr}[(f\,\theta'-f'\,\theta)-A\,e^{-X}(4\theta+\eta\,\theta')+H\,f'^2]+A_1f'+B_1\theta=0 \tag{9}$$

$$\phi''+Sc\ [(f\,\phi'-f'\,\phi)-A\,e^{-X}(4\phi+\eta\,\phi')]=0 \tag{10}$$

the reduced boundary conditions are as follows:

$$f(0)=S,f'(0)=1,\theta(0)=1,\ \phi(0)=1\ \ \text{at}\,\eta=0$$
$$f'(\infty)\to 0,\theta(\infty)\to 0,\phi(\infty)\to 0\quad \text{as}\ \ \eta\to\infty \tag{11}$$

where $We = \Gamma\sqrt{\frac{U^3}{\nu\, L}}$ is the Weissenberg number, $A = \frac{\alpha L}{U_0}$ is the unsteadiness parameter, $X = \frac{x}{L}$ is the dimensionless coordinate, $M = \frac{2L\sigma\, B_0^2}{\rho\, U_o}$ is the magnetic parameter, $\mathrm{Pr} = \frac{\rho\, C_p \nu}{\kappa}$ is the Prandtl number, $H = M.Ec$ is the joule heating parameter, $Sc = \frac{\nu}{D_m}$ is the Schmidt number, $\mathrm{S} = \frac{V_0}{\sqrt{\frac{U_0\,\nu}{2L}}}$ suction or blowing parameter, and the prime denotes the differentiation w. r. t. η.

The Skin-friction coefficient, Nusselt number, and Sherwood number, which are the physical quantities of interest in this problem, are defined by

$$C_f = \frac{2\,\tau_w}{\rho\, U^2} = \sqrt{\frac{2x}{L}}\ (Re_x)^{-\frac{1}{2}} f''(0) \tag{13}$$

$$N_{u_x} = \frac{x\, q_w}{k(T_w - T_\infty)} = -\sqrt{\frac{x}{2\,L}}\ \sqrt{Re_x}\ \theta'(0) \text{ and} \tag{14}$$

$$S_{h_x} = \frac{\mathrm{x\,J_w}}{\mathrm{D}\,(C_w - C_\infty)} = -\sqrt{\frac{x}{2\,L}}\ \sqrt{Re_x}\ \phi'(0) \tag{15}$$

3. Results and Discussion

A Williamson fluid's boundary layer flow, heat, and mass transfer over an exponentially stretching sheet are considered. The reduced non-linear ordinary differential equations (8) - (10) subject to the boundary conditions (11) are solved numerically with bvp4c solver, which is programmed in MATLAB software. The following parameters remain fixed throughout the study unless otherwise stated:

$X = 2, \psi = \frac{\pi}{2}, We = 0.1, M = 0.2, A = S = 0.5, Pr = 3, H = A_1 = B_1 = 0.3\ \ and\ \eta = 1.5.$

We describe the result attained in this work through Figs. 1-23. The computed values of skin friction coefficient, Nusselt, and Sherwood number for various governing parameters are presented in tables 1, 2, and 3.

3.1. *Velocity profile*

Figs. 1-5 illustrates the variation of fluid velocity for different values governing parameters. Fig. 1 displays the effects of an aligned angle (ψ) on velocity graph. It is observed that the velocity profile decreases with rising values of aligned angle (ψ). Fig. 2 is plotted to examine the influence of the Weissenberg number on the velocity profile. It is noticed that fluid velocity is a decreasing function of the Weissenberg number (We). The ratio of relaxation time to specific process time is termed the Weissenberg number. The specific process time decreases due to the Weissenberg number. Decreasing specific process time reduces fluid velocity along with the boundary layer thickness. Fig. 3 describes the impact of magnetic parameters on velocity distribution. We see that fluid

temperature decreases with increasing values of the magnetic parameter (M). Physically, a drag-like force known as the Lorentz force formed by the magnetic field opposes the motion of the fluid and, therefore, reduces the velocity of the fluid. Fig. 4 exhibits an increase in the unsteadiness parameter (A) causes augmentation in the velocity field as well as momentum boundary layer thickness. Fig. 5 depicts the effect of the suction parameter on the velocity profile. It is noted that fluid velocity reduces with rising values of the suction parameter $(S > 0)$ whereas fluid velocity is seen to increase with blowing parameter $(S < 0)$.

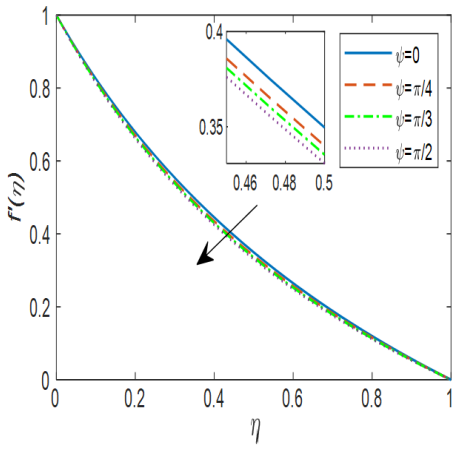

Fig. 1. Velocity profile for different values of alinged angle (ψ).

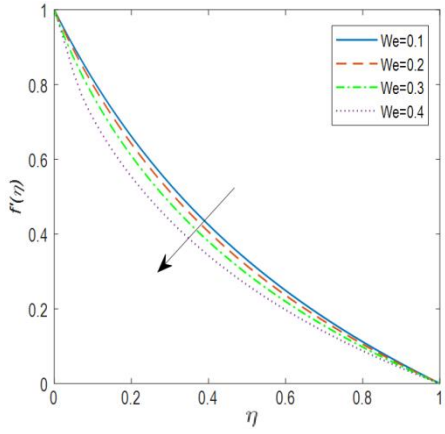

Fig. 2. Velocity profile for different values of Weissenberg number (We).

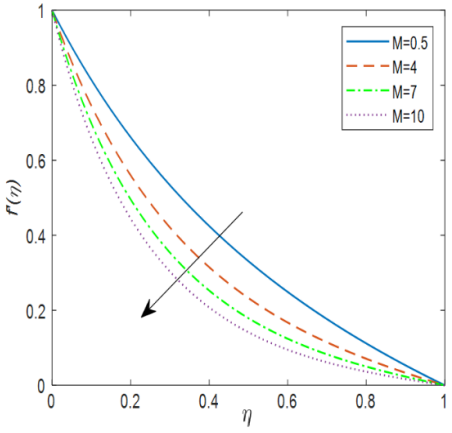

Fig. 3. Velocity profile for different values of magnetic parameter (M).

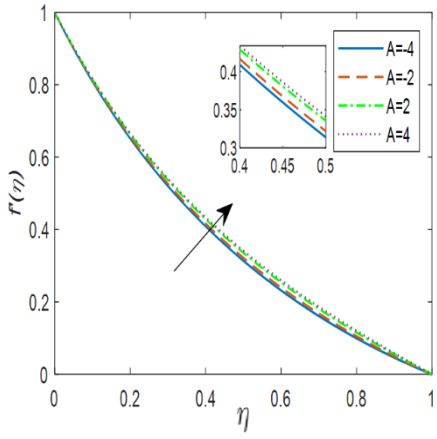

Fig. 4. Velocity profile for different values of unsteadiness parameter (A).

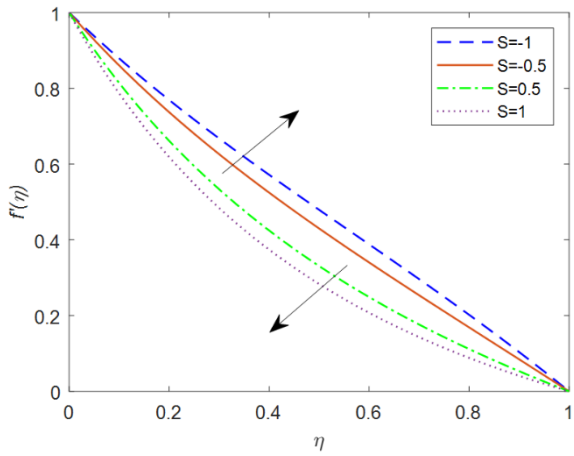

Fig. 5. Velocity profile for different values of suction or blowing parameter.

3.2. *Temperature profile*

The influences of different non-dimensional governing parameters on fluid temperature are shown in Figs. 6-13. Figure 6 is drawn to demonstrate the effect of Weissenberg number (We) on the temperature profile. It is seen from the figure that fluid temperature accelerates due to the increase in Weissenberg number (We). It is observed from Fig. 7 that the temperature profile is an increasing function of the magnetic parameters. Fig. 8 illustrates the effect of the unsteadiness parameter on the temperature profile, and we notice that the temperature profile descends with the enlargement of the unsteadiness parameter. This is physically so because increasing the unsteadiness enhances heat loss due to the stretching of the sheet, thus decreasing the temperature profile. This implies that the rate of cooling is much faster than the rate of cooling for the steady flow because of the decrease in the heat transfer rate from the sheet to the fluid for higher values of the unsteady parameter. Fig. 9 reveals the effect of Prandtl number (Pr) on the temperature profile. The ratio of momentum diffusivity to thermal diffusivity is termed as the Prandtl number. It is apparent to us that augmentation in thermal diffusivity turns a decrease in the Prandtl number, which reduces the fluid temperature. Fig. 10 is a sketch to interpret the impact of the joule heating parameter (H) on the temperature field. The mechanical energy is transformed into thermal energy because of the inside friction of molecules, and as a result, temperature increases. The effect of suction/blowing on the temperature field is presented in Fig. 11. We can conclude from the figure that fluid temperature is smaller in suction than blowing. Figs. 12 and 13 explore the influences of heat generation parameters $(A_1, B_1 > 0)$ or heat absorption parameters $(A_1, B_1 < 0)$ on the temperature profile. The thermal boundary layer produces energy for which the temperature field enhances with rising values of $A_1, B_1 > 0$. On the other hand, the boundary layer energy is absorbed when $A_1, B_1 < 0$, and therefore, the fluid temperature reduces with diminishing values of $A_1, B_1 < 0$.

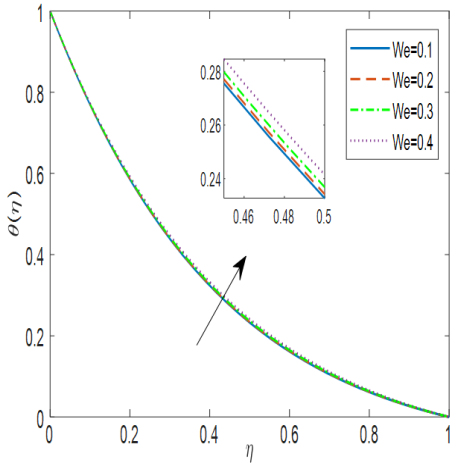

Fig. 6. Temperature profile for different values of Weissenberg number (We).

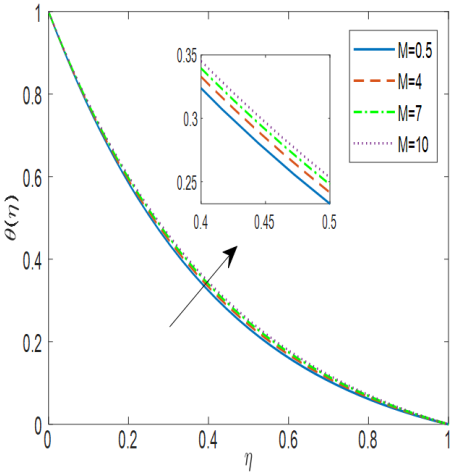

Fig. 7. Temperature profile for different values of magnetic parameter (M).

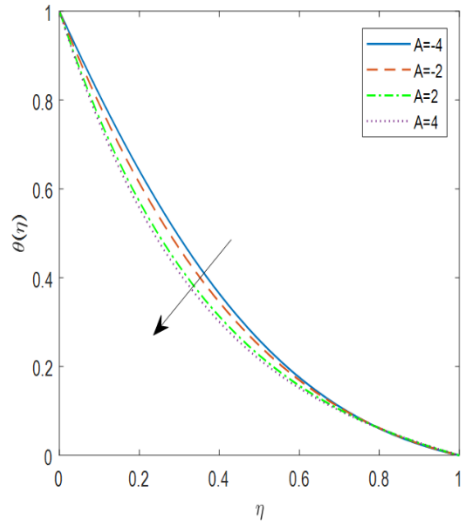

Fig. 8. Temperature profile for different values of unsteadiness parameter (A).

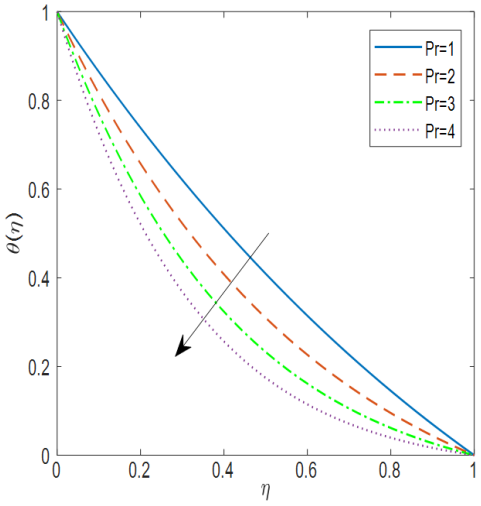

Fig. 9. Temperature profile for different values of Prandtl number (Pr).

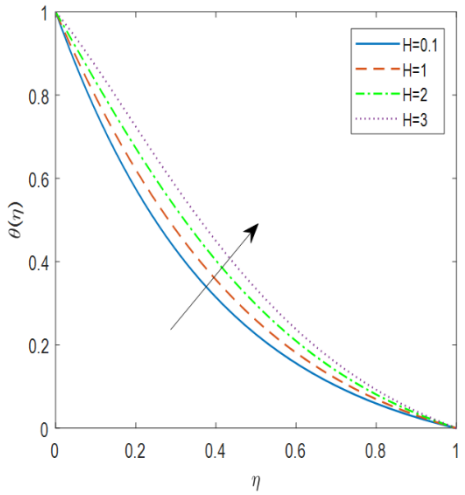

Fig. 10. Temperature profile for different values of joule heating parameter (H).

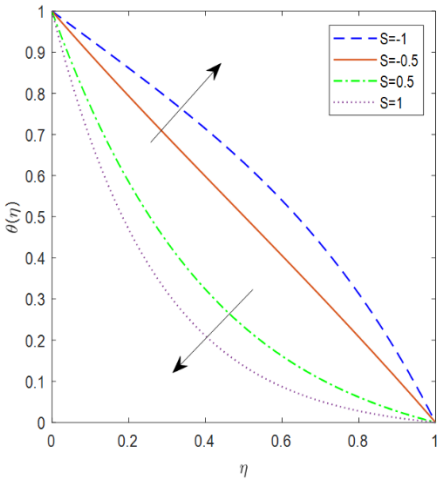

Fig. 11. Temperature profile for different values of suction or blowing parameter (S).

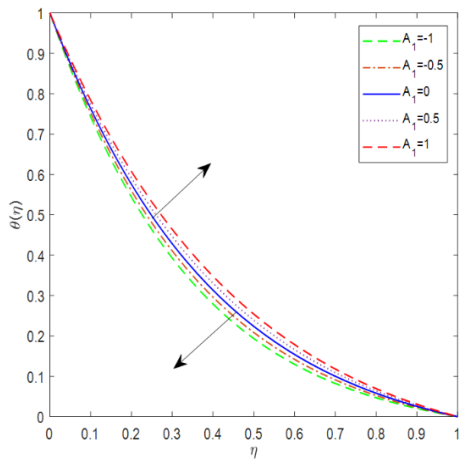

Fig. 12. Temperature profile for different values of heat generation/ absorption parameter (A_1).

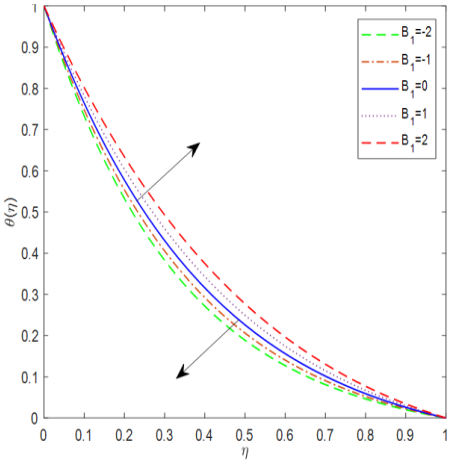

Fig. 13. Temperature profile for different values of heat generation/ absorption parameter (B_1).

3.3. *Concentration profile*

Figs. 14-18 exhibits concentration profiles for different values of non-dimensional governing parameters. Fig. 14 is portrayed to examine the effect of Weissenberg number (We) on concentration profile. It is seen that the concentration profile increases as We increases. Fig. 15 describes the effect of the magnetic parameter (M) on concentration profile. It is observed that the concentration field enhances with the increment of M. Impression of unsteadiness parameter (A) on the concentration profile is displayed in figure 16. It is revealed that an augmentation in the unsteadiness parameter declines the

concentration distribution. Fig. 17 indicates that increasing Schmidt's number (Sc) concentration profile gets decreasing curve. The Schmidt number (Sc) is inversely proportional to mass diffusivity which leads a reduction in the concentration profile. Fig. 18 represents the profile of concentration for different values of suction $(S > 0)$/ blowing $(S < 0)$ parameter. It is noticed that the concentration profile ascends towards the suction $(S > 0)$ parameter while it is descending toward blowing $(S < 0)$ parameter.

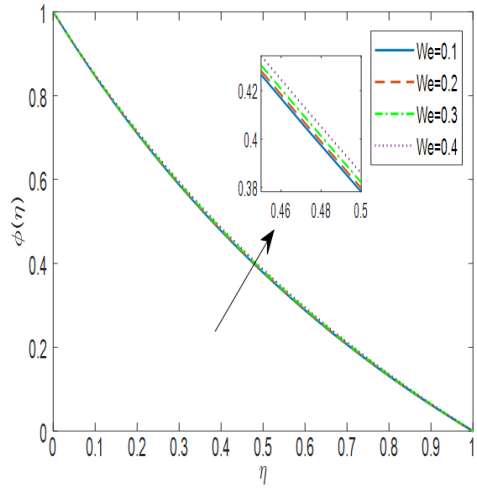

Fig. 14. Concentration profile for different values of Weissenberg number (We).

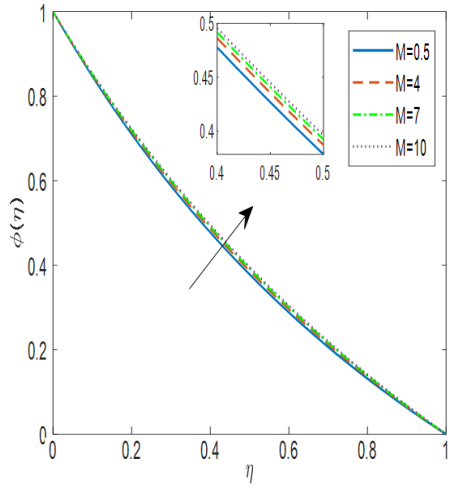

Fig. 15. Concentration profile for different values of magnetic parameter (M).

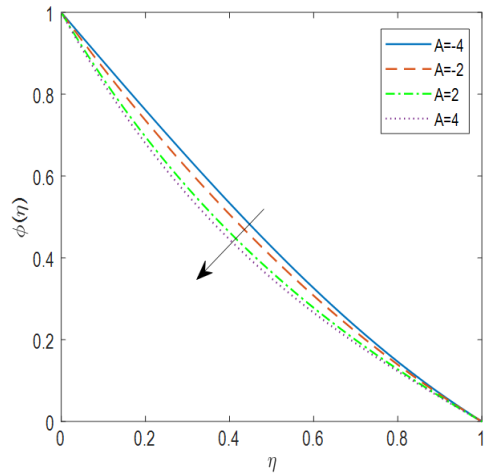

Fig. 16. Concentration profile for different values of unsteadiness parameter (A).

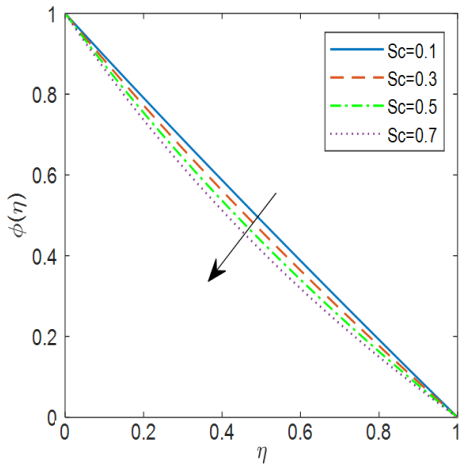

Fig. 17. Concentration profile for different values of Schmidt number (Sc).

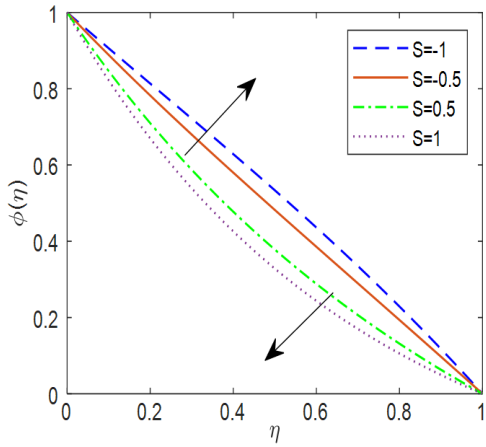

Fig. 18. Concentration profile for different values of suction or blowing parameter.

3.4. *Skin friction coefficient, Nusselt, and Sherwood number*

Figs. 19-23 shows the impacts of Weissenberg number, joule heating parameter, non-uniform heat generation, and absorption parameter on important engineering coefficients. Fig. 19 examines the effect of Weissenberg number (We) on shear stress. It is noted that shear stress reduces initially, but after a certain distance η from the stretching sheet, it enhances gradually. The variation of the joule heating parameter (H) on the temperature gradient is shown in Fig. 20. We can see from Fig. 20 that the temperature gradient accelerates initially, but after a certain distance η from the stretching sheet, it decelerates gradually. Similarly, the temperature gradient accelerates initially with a non-uniform heat generation parameter $(A_1 > 0)$ but after a certain distance η from the stretching sheet, it decelerates gradually, whereas is opposite nature is observed for the non-uniform heat absorption parameter $(A_1 < 0)$. These results are plotted in Figs. 21 and 22. Fig. 23 elucidates the influence of the Schmidt number on the mass transfer rate. We notice that the mass transfer rate decreases initially, but after a certain distance η from the stretching sheet, it increases gradually.

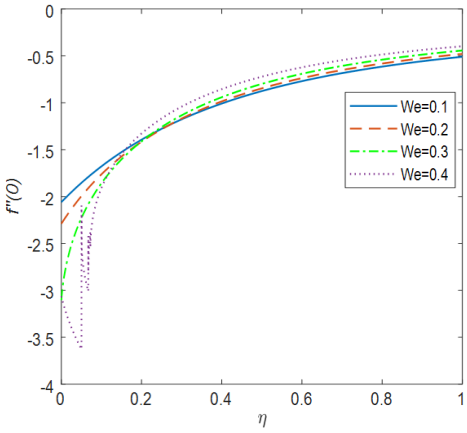

Fig. 19. Concentration profile for different values of suction or blowing parameter.

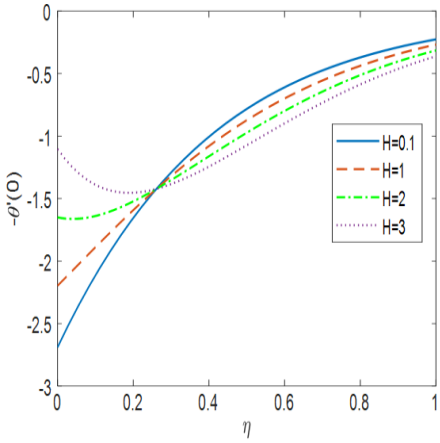

Fig. 20. Concentration profile for different values of suction or blowing parameter.

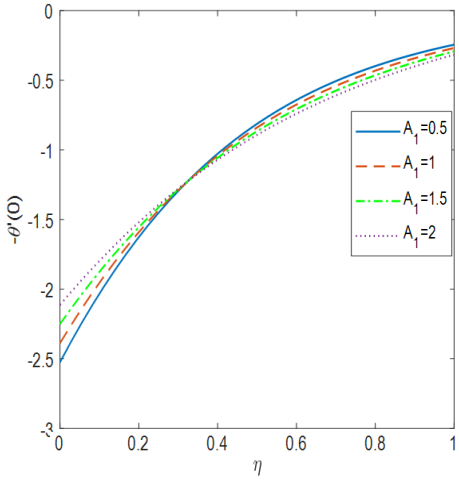

Fig. 21. Temperature gradient for different values of heat generation parameter ($A_1 > 0$).

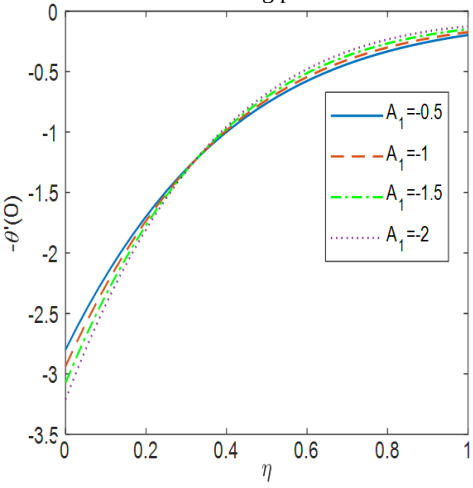

Fig. 22. Temperature gradient for different values of heat absorption parameter ($A_1 < 0$).

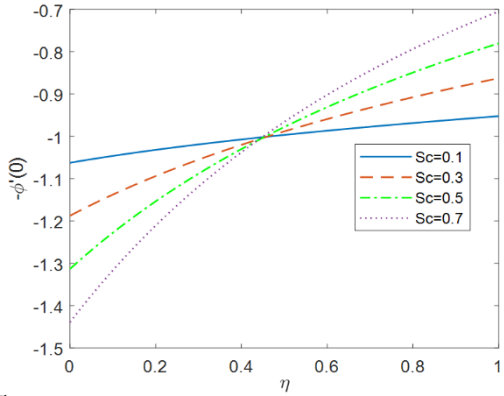

Fig. 23. Concentration gradient for different values of Schmidt number (Sc).

3.5. *Table discussion*

Tables 1-3 show the effect of various parameters on the surface drag coefficient, heat transfer, and mass transfer rates. From Table 1, we observe an augmentation in the values of the aligned angle (ψ), Weissenberg number (We), magnetic parameter (M) and suction parameter $(S > 0)$ makes a decrement in the skin friction coefficient, but an increment in the skin friction coefficient is seen for a rise in the values of the unsteadiness parameter (A). From Table 2, it is noticed that an improvement in the values of the aligned angle (ψ), Weissenberg number (We), magnetic parameter (M), joule heating parameter (H), heat generation parameters $(A_1, B_1 > 0)$ brings about an abatement in the heat transfer rate but an increase in the values of the unsteadiness parameter (A) leads to an enhancement in the heat transfer rate. From Table 3, we know that the mass transfer rate enhances due to an escalation in the values of the Prandtl number (Pr) but reduces because of H, A_1 and B_1.

4. Conclusion

Two-dimensional unsteady flow of Williamson fluid with suction or blowing in the presence of joule heating, non-uniform heat generation or absorption, and inclined magnetic field over an exponentially stretching sheet is investigated. Non-linear ordinary differential equations are obtained from governing partial differential equations using similarity transformation. The impacts of different non-dimensional parameters on the flow field are illustrated through graphs and tables. We list the main findings of this article as follows:

- The increasing Weissenberg number decelerates the fluid velocity, while an opposite trend is seen for temperature and concentration distributions.
- The fluid velocity reduces due to an improvement in the aligned angle.
- The velocity profile reduces, whereas the temperature and concentration profile increase with the rising values of the magnetic parameter.
- The unsteadiness parameter amplifies fluid velocity and depreciates fluid temperature and concentration.
- The joule heating parameter boosts the temperature field.
- The generation parameters accelerate fluid temperature, whereas the heat absorption parameters decelerate fluid temperature.

Table 1. Skin friction coefficient for different values of ψ, We, M, A, Pr, S.

Parameter	Values	$f''(0)$
ψ	$\frac{\pi}{4}$	-1.9842
	$\frac{\pi}{3}$	-2.0215
	$\frac{\pi}{2}$	-2.0586
We	0.2	-2.2891
	0.3	-3.1040
	0.4	-3.0607
M	4	-3.0024
	7	-3.7143
	10	-4.3794
A	-2	-2.0887
	2	-2.0446
	4	-2.0296
S	-1	-1.2767
	-0.5	-1.4928
	1	-2.4207

Table 2. Nusselt number for different values of $\psi, We, M, A, Pr, S, A_1, B_1, H$.

Parameter	Values	$-\theta'(0)$
ψ	$\frac{\pi}{4}$	2.5778
	$\frac{\pi}{3}$	2.5761
	$\frac{\pi}{2}$	2.5744
We	0.2	2.5666
	0.3	2.5520
	0.4	2.5252
M	4	2.5307
	7	2.4983
	10	2.4702
A	-2	2.2703
	2	2.7156
	4	2.8676
S	-1	0.6925
	-0.5	1.0727
	1	3.6806
A_1	-0.5	2.7903
	0	2.6554
	0.5	2.5205
$B_{1.}$	-1	2.8623
	0	2.6436
	1	2.4059
Pr	1	1.4027
	2	1.9927
	4	3.1422
H	0.1	2.6805
	1	2.2031
	2	1.6727

Table 3. Sherwood number for different values of ψ, We, M, A, S, Sc.

Parameter	Values	$-\phi'(0)$
ψ	$\frac{\pi}{4}$	1.6316
	$\frac{\pi}{3}$	1.6300
	$\frac{\pi}{2}$	1.6284
We	0.2	1.6216
	0.3	1.6102
	0.4	1.5909
M	4	1.5920
	7	1.5693
	10	1.5514
A	-2	1.4120
	2	1.7401
	4	1.8721
S	-1	0.9491
	-0.5	1.1417
	1	1.9232
Sc	0.1	1.0623
	0.3	1.1874
	0.5	1.3130

References

1. S. Shateyi and H. Muzara, Computation **8**, 55, (2020). https://doi.org/10.3390/computation8020055
2. M. J. Babu and N. Sandeep, Alexandria Eng. J. **5**, 2193 (2016). http://dx.doi.org/10.1016/j.aej.2016.06.009
3. Z. Shah, E. Bonyah, S. Islam, W. Khan, and M. Ishaq, Heliyon **4** (2018). https://doi.org/10.1016/j.heliyon.2018.e00825
4. L. A. Lund, Z. Omar, and I. Khan, Heliyon, **5** (2019). https://doi.org/10.1016/j.heliyon.2019.e01345
5. T. Salahuddin, M. Khan, T. Saeed, M. Ibrahim, and Y. M. Chu, Case Studies in Thermal Eng. **25**, ID 100895 (2021). https://doi.org/10.1016/j.csite.2021.100895
6. R. Ellahi, Appl. Math. Model. **37**,1451 (2013). https://doi.org/10.1016/j.apm.2012.04.004
7. R. Ellahi, S. Z. Alamri, A. Basit, and A. Majeed, J. Taibah University Sci. **12**, 476 (2018). https://doi.org/10.1080/16583655.2018.1483795
8. N. Shehzad, A. Zeeshan, M. Shakeel, R. Ellahi, and S. M. Sait, Coatings **12**, 430 (2022). https://doi.org/10.3390/coatings12040430
9. T. Sajid, S. Tanveer, Z. Sabir, and J. L.G. Guirao, Math. Problems Eng. **2020** (2020). https://doi.org/10.1155/2020/5251804
10. J. K. Madhukesh, G. K. Ramesh, E. H. Aly, and A. J. Chamkha, Alexandria Eng. J. **61**, 2418 (2022). https://doi.org/10.1016/j.aej.2021.06.104
11. D. Srinivasacharya and P. Jagadeeshwar, Math. Sci. **13**, 201 (2019). https://doi.org/10.1007/s40096-019-0290-8

12. A. Sinha, J. C. Misra, and G. C. Shit, Alexandria Eng. J. **55**, 2023 (2016). https://doi.org/10.1016/j.aej.2016.07.010
13. B. K. Swain, B. C. Parida, S. Kar, and N. Senapati, Heliyon, **6**, ID e05338 (2020). https://doi.org/10.1016/j.heliyon.2020.e05338
14. T. Hayat, A. Shafiq, M. A. Farooq, H. H. Alsulami, and, S. A. Shehzad, J. App. Fluid Mechanics, **9**, 1969 (2016). https://doi.org/10.18869/acadpub.jafm.68.235.24646
15. K. Sharada and B. Shankar, Glob J. Pure Appl. Math. **13**, 5965 (2017).
16. A. Hamid, M. Khan, and A. Hafeez, Inter. J. Heat and Mass Transfer **126**, 933 (2018). https://doi.org/10.1016/j.ijheatmasstransfer.2018.05.076
17. S. Mukhopadhyay, Ain Shams Eng. J. **4**, 485 (2013). http://dx.doi.org/10.1016/j.asej.2012.10.007
18. M. A. Islam, M. Y. Ali, and S. M. O. Gani, J. Sci. Res. **2**, 14 (2022). http://dx.doi.org/10.3329/jsr.v14i2.55577
19. M. A. Islam, M. Y. Ali, R. Akter, and S. M. O. Gani, J. App. Math. Phys. **10**, 3016 (2022). https://doi.org/10.4236/jamp.2022.1010202
20. G. R. Rajput, B. P. Jadhav, V. S. Patil, and S. N. Salunkhe, Heat Transfer, **50**, 2543 (2021). https://doi.org/10.1002/htj.21991